Tectonophysics 744 (2018) 322–332

Contents lists available at ScienceDirect

Tectonophysics

journal homepage: www.elsevier.com/locate/tecto

Stress transfer and connectivity between the Bhutan Himalaya and the Shillong Plateau

Djordje Grujic[a,*], György Hetényi[b], Rodolphe Cattin[c], Saurabh Baruah[d], Angélique Benoit[c], Dowchu Drukpa[e], Adi Saric[a]

[a] Department of Earth Sciences, Dalhousie University, PO BOX 15000, Halifax, Canada
[b] Institute of Earth Sciences, University of Lausanne, UNIL-Mouline Géopolis, Lausanne, Switzerland
[c] Géosciences Montpellier, Université de Montpellier, Montpellier, France
[d] Geoscience and Technology Division, CSIR-North East Institute of Science and Technology, Jorhat 785006, Assam, India
[e] Seismology and Geophysics Division, Department of Geology and Mines, Thimphu, Bhutan

ARTICLE INFO

Keywords:
Coulomb stress change
Stress transfer
Bhutan Himalayas
Shillong Plateau
Seismotectonics

ABSTRACT

Within the northern Indian Plate, the Shillong Plateau is a peculiar geodynamic terrane, hosting significant seismic activity outboard the Himalayan belt. This activity is often used as an argument to explain apparent reduced seismicity in the Bhutan Himalayas. Although current geophysical and geodetic data indicate that the Bhutan Himalayas accommodate more deformation than the Shillong Plateau, we aim to quantify the extent to which the two geodynamic regimes are connected and potentially interact through stress transfers. We compiled a map of major faults and earthquakes in the two regions and computed co-seismic stress transfer amplitudes. Our results indicate that the Bhutan Himalayas and the Shillong Plateau are less connected than previously suggested. Major earthquakes in either of the two regions mainly affect transverse faults connecting them, causing up to ~40 bar Coulomb stress change; however, this effect is clearly less on thrust faults of the either region (up to 1 bar only). The M_W 8.25 1897 Assam earthquake that affected the Shillong Plateau did not cause a stress shadow on the Main Himalayan Thrust in Bhutan as previously suggested. Similarly, the Mw 8 ± 0.5 1714 Bhutan earthquake had negligible impact on stress accumulation on thrust faults bounding the Shillong Plateau. Furthermore, the main process shaping the regional stress patterns continues to be interseismic loading with complex boundary conditions in a diffuse deformation field involving the Bengal Basin and Indo-Burman Ranges. While both the Bhutan Himalayas and the Shillong Plateau exhibit a compressional regime, their stress evolutions are more weakly connected than hypothesized. Although our modelling suggests lateral increase in stress interactions, from west (less) to east (more), in the Bhutan Himalayas, a clearer picture will only emerge with better constrained fault geometries, slip rates, crustal structure, and seismicity catalogues in the entire region of distributed deformation.

1. Introduction

The active tectonics of the eastern Himalayas is distinct from that of the rest of the Himalayan orogen due to their distributed deformation zone, which also encompasses the Shillong Plateau and the Indo-Burman Ranges. The main characteristics of the Bhutan Himalayas are as follows:

1. The western Bhutan Himalayas were affected by an Mw 7.5–8.5 earthquake in 1714 (Berthet et al., 2014; Hetényi et al., 2016b; Le Roux-Mallouf et al., 2016). However, according to instrumental records, there appears to be less moderate earthquake activity in Bhutan than in Nepal, with a locked Main Himalayan Thrust (MHT) in western Bhutan and a seismically active MHT in eastern Bhutan (Diehl et al., 2017; Marechal et al., 2016).
2. The Bhutan and Darjeeling–Sikkim Himalayas, as well as their foreland basin (which includes the Brahmaputra valley), are affected by a dominantly strike-slip deformation in a generally contractional tectonic setting (e.g., Drukpa et al., 2006; Velasco et al., 2007; Diehl et al., 2017). During the last century, a seismic event exceeding M 7 affected the Brahmaputra valley and several $M > 6$ events have been registered in the eastern Himalayas.
3. The Shillong Plateau to the south of Bhutan is the only elevated terrain outside of the entire Himalayan orogen and is bound to the

* Corresponding author.
E-mail address: dgrujic@dal.ca (D. Grujic).

https://doi.org/10.1016/j.tecto.2018.07.018
Received 17 December 2017; Received in revised form 27 June 2018; Accepted 24 July 2018
Available online 26 July 2018

north and south by conjugate reverse faults. It was affected by one of the largest known intraplate earthquakes in 1897 (England and Bilham, 2015).

The seismotectonics of the Himalayas are controlled by slip along the basal décollement of the orogen, the Main Himalayan Thrust (MHT). The structure emerges at the surface as the Main Frontal Thrust (MFT), which forms the boundary between the deforming Himalayan foothills and the flexural Indus–Ganges–Brahmaputra foreland basin above the rigid Indian Plate (Berthet et al., 2013; Hammer et al., 2013). Modelling of interseismic data on the Nepal Himalayas (Cattin and Avouac, 2000) suggests that the MHT is locked during the interseismic period from the trace of the MFT to ~100 km down dip. This process results in stress build-up, triggering the seismic activity observed in Nepal in a belt about 100 km north from the MFT trace.

This pattern slightly changes to the east of Sikkim. A narrow, dextral, mid- to deep-crustal strike-slip seismicity belt, the Dhubri-Chungthang Fault (DCF) zone breaks the Indian Plate as it extends from the NW corner of Sikkim, across the Brahmaputra basin, to the NW corner of the Shillong Plateau (Diehl et al., 2017). This belt was probably responsible for the 1930 Mw 7.1 ± 0.4 Dhubri earthquake (Gee, 1934, ISC-GEM catalogue, version 5 http://www.isc.ac.uk/iscgem/). A similar, but more diffuse strike-slip seismic belt, the Kopili Fault zone extends along the eastern border of the Shillong Plateau and into SE Bhutan (e.g., Hetényi et al., 2016a; Kumar et al., 2015; Sutar et al., 2017). Both seismic zones have no associated surface or geological deformation, although they are seismically more active than the thrust faults. In contrast, the conjugate, sinistral, strike-slip faults Lingshi and Sakteng (Gansser, 1983; our observations) appear to affect only the orogenic wedge and have clear geological offsets (Long et al., 2011). Apart from these faults, the deformation of the orogenic wedge in the western Bhutan Himalayas seems to be similar to that in the central Himalayas, with a locked flat segment of the MHT (Marechal et al., 2016) and with microseismicity recorded in the area of the ramp along the MHT (Diehl et al., 2017). However, the eastern Bhutan Himalayas are unique because, in this region, the flat segment of the MHT appears to be creeping geodetically (Marechal et al., 2016) and has been seismically active (Diehl et al., 2017). Furthermore, compared with the Nepal Himalayas, the crust beneath the Bhutan Himalayas has a lower flexural rigidity (Hammer et al., 2013). According to paleoseismic evidence and historical records, the last major earthquake in Bhutan with Mw 8.0 ± 0.5 occurred in May 1714 (Hetényi et al., 2016b; Le Roux-Mallouf et al., 2016) and potentially ruptured the MHT along most of the Bhutan Himalayas.

The area to the south of Bhutan was affected by the “great Assam earthquake” of 1897 with Mw 8.1–8.25 (Bilham and England, 2001), traditionally interpreted as the largest known continental intraplate earthquake. The slip occurred along the geodetically inferred Oldham Fault (England and Bilham, 2015), a south-dipping, reverse, blind fault that has not been identified in the field (Rajendran et al., 2004). The southern boundary of the Shillong Plateau is the Dauki Fault, a moderately northward-dipping, reverse fault with an ~10-km throw (Biswas et al., 2007), and slip along this fault has been suggested to partition up to one third of the India–Asia convergence (Bilham and England, 2001). Stress interactions between the Himalayan orogen and the Shillong Plateau are expected to exist on geological timescales because reverse slip on the Dauki Fault started during the late Miocene (Biswas et al., 2007; Clark and Bilham, 2008).

Five models have been proposed for the Shillong Plateau formation, all of which are variations of the formation of basement-cored uplifts (aka arches) in the orogenic foreland (Weil and Yonkee, 2012; Yeck et al., 2014). The first model proposes uplift along the frontal ramp of the subhorizontal Himalayan basal detachment extending south underneath the Shillong Plateau (Molnar, 1987; Molnar and Pandey, 1989; Oldham, 1899; Seeber and Armbruster, 1981). However, currently, no seismicity pattern suggesting the existence of an active décollement beneath Brahmaputra Basin has been noted (Diehl et al., 2017; Singer et al., 2017; Marechal et al., 2016). The second model proposes the formation of a pop-up structure (Bilham and England, 2001), involving a pair of conjugate crustal-scale faults with nearly equivalent finite displacement. The force driving this deformation is the bending of the Indian Plate by the combined weight of the Himalayas in the north and the Bengal fan deposits in the south. The third model proposes fold hinge migration (Clark and Bilham, 2008) in which the Oldham Fault is the principal structure formed by the growth of a crustal anticline and northward migration of its hinge (NB: Clarke and Bilham have labelled the fold axis instead of the fold axial surface.). This model also proposes that the Shillong fault system is the manifestation of the fragmentation of the Indian plate. The fourth model proposes a northward tilting of the Indian crust (Biswas et al., 2007); according to this model, the Dauki Fault is the only structure responsible for the rise of the Shillong Plateau, with negligible displacement along the Oldham Fault. The fifth model proposes a self-consistent jump of deformation into the orogenic foreland (Jaquet et al., 2017). This generic numerical model of collisional orogenic wedges predicts formation of first- and second-order shear zones by thermal softening, local temperature increase due to shear heating, and temperature dependence of viscosity.

Thus, the unique seismotectonic setting in the Himalayas raises several questions regarding interaction between the Bhutan Himalayas and the Shillong Plateau. Here we address three issues:

1. The effect of the 1897 Assam earthquake on the MHT
2. The effect of the 1714 Bhutan earthquake on the faults bounding the Shillong Plateau
3. The regional stress interaction between plates and their fragments

Although a recent study on Coulomb stress transfer (Gahalaut et al., 2011) has indicated that the 1897 Assam earthquake caused a stress shadow in the Bhutan Himalayas and a “seismic gap” along the Himalayan seismic belt, new information concerning this rupture (England and Bilham, 2015) as well as new GPS data, seismic data, and paleoseismic results on Bhutan (e.g., Berthet et al., 2014; Diehl et al., 2017; Hetényi et al., 2016b; Le Roux-Mallouf et al., 2016; Marechal et al., 2016; Vernant et al., 2014) require revisiting the interaction between the Himalayan orogen and the Shillong Plateau.

To address these questions, in this study, we performed calculations of co-seismic Coulomb and normal stress transfer between the source faults and receiver faults that we compiled for the region encompassed by the Bhutan Himalayas and the Shillong Plateau. We accounted for numerous scenarios involving three historical $M > 7$ earthquakes, known and inferred interseismic slip rates, and a range of values of Young's modulus and Poisson's ratio. We also compared seismic stress transfer and interseismic stress loading to obtain an estimate of the number of years by which earthquakes have been “delayed” or “advanced” by preceding events. Because of a lack of data, we neglected postseismic slip or downdip creep in dip-slip faults, thus probably underestimating the total stress transfer during an event. Furthermore, we omitted postseismic asthenospheric and lower crustal relaxations transferring stress to the upper crust.

2. Methods

2.1. Active faults

We built a network of 13 faults based on our field knowledge, information in the literature, and discussions with a number of colleagues (Figs. 1 and S1). We used our recent geophysical (seismological and GPS) and field observations to constrain the geometry and kinematics of these active faults as well as the crustal mechanical parameters required for calculations of co-seismic stress transfer (all the data and the related references are shown in Table S1 in the Supporting information). This

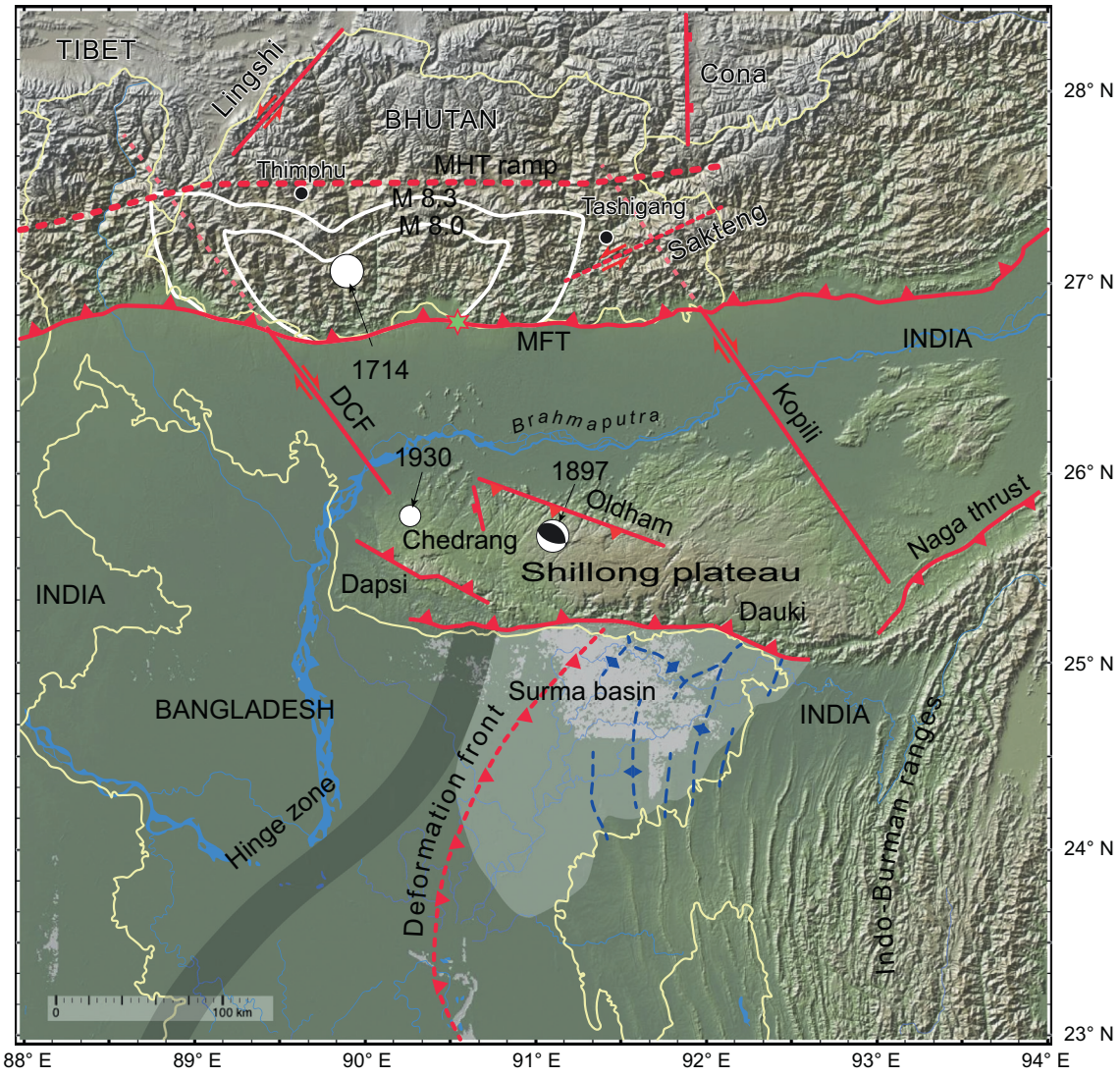

Fig. 1. Network of faults investigated in this study. Digital elevation model of the eastern Himalayas and its foreland with the traces of the studied structures. The Lingshi and Sakteng faults are from the geological map of Gansser (1983) and our observations. Fault traces are depicted in red, and those shown as dashed lines indicate that the seismogenic fault has no surface trace. Dashed fault traces in pink indicate that the seismogenic fault is beneath the Himalayan orogenic wedge. The likely epicentres of the major earthquakes investigated in this paper are also shown on the map: 1714, *Mw* 8 ± 0.5 (Hetényi et al., 2016b); 1897, *Mw* 8.25 ± 0.1 (England and Bilham, 2015); 1930, *Mw* 7.1 (Gee, 1934; Szeliga et al., 2010). White contours indicate the presumed hypocentre location of the 1714 earthquake along the MHT (Hetényi et al., 2016b), and the star indicates the surface break along the MFT caused by the same event (Le Roux-Mallouf et al., 2016). The Indian crust to the east of the "hinge zone" and south of the Dauki Fault is a thinned transitional or oceanic crust (Alam et al., 2003; Salt et al., 1986). The deformation front (shown as a red dashed curve) is a blind thrust of the Indo-Burman Ranges (Steckler et al., 2016). The darker blue lines in the Surma Basin represent hinges of buried anticlines (Najman et al., 2016) within the same accretionary wedge.

structural model contains all the known first-order active faults in the study area; it includes more faults than discussed in this paper. However, a study by Lin and Stein (2004) demonstrated that, in addition to source fault geometry, receiver fault geometry is highly important in Coulomb stress modelling.

Faults other than the Dauki Fault, the Oldham Fault, the DCF, and the MHT have not been imaged geophysically and some of them have no surface expression; therefore, their geometry at depth is uncertain to various degrees. Because of inadequate structural information at depth to test models for the Shillong Plateau formation, we adopted a kinematic model in which the plateau is bounded by two steep conjugate reverse faults. Hence, hereinafter, for all faults besides the MHT (see Section 3.1), we will assume planar fault geometry (Fig. S1) for the sake of simplicity.

2.2. Coulomb stress change

We performed a series of calculations of co-seismic stress changes where one of the major faults acted as the "source" fault along which slip occurred, and all the other faults were the "receiver" faults upon which the resolved stress was investigated. We assumed that seismic rupture plane orientation is mainly controlled by geological structures rather than by the co-seismic and regional stress field. Furthermore, we favoured failure plane orientation controlled by geological fault planes, and thus explored receiver faults with geometry as inputs. Planes optimally oriented for failure, derived from the regional stress field, and an assumed friction coefficient (e.g., King et al., 1994; Ma et al., 2005) were used in our study for comparison. We considered three faults related to major modern or historical earthquakes as source faults: the Oldham Fault, the MHT, and the DCF. Despite about 10 km of vertical displacement along the Dauki fault since 9–15 Ma (Biswas et al., 2007),

and geological evidence for ongoing slip (Vernant et al., 2014; Barman et al., 2016) there is no evidence yet for a major paleoseismic event along the Dauki fault. Low angle reverse faults and paleo-liquefaction phenomena in the area that have been dated (Sukhija et al., 1999; Morino et al., 2011) cannot be reliably related to the source fault. Consequently, we modeled only a hypothetical earthquake along this fault (Fig. S7). For 1897 event related to the Oldham Fault, slipped area, average slip, and rake were constrained by geodetic data (England and Bilham, 2015), whereas for events related to the latter two faults, the approximate rupture size was derived according to empirical scaling by Wells and Coppersmith (1994), and the average slip was calculated to yield the estimated magnitude.

The calculations were performed using the USGS Coulomb v.3.4 software (Lin and Stein, 2004; Toda, 2005). To calculate static stress change, we assumed dislocations embedded in an elastic half-space with a Young's modulus E and a Poisson's ratio ν. The Coulomb stress change is given as

$$\Delta CFS = \Delta\tau + \mu\Delta\sigma_n \quad (1)$$

where $\Delta\tau$, $\Delta\sigma_n$, and μ are the shear stress change, the normal stress change ($\Delta\sigma_n < 0$, clamping or $\Delta\sigma_n > 0$, unclamping of a fault), and the effective friction coefficient, respectively. We performed calculations with $\nu = 0.25$ for three values of the friction coefficient—$\mu = 0.2$, 0.4, and 0.8—and for three values of the Young's modulus—$E = 50$, 80, and 100 GPa (Hammer et al., 2013)—to account for possible scenarios (Supporting information Fig. S2). The influence of regional stress [direction, as derived from the regional GPS data (Marechal et al., 2016; Vernant et al., 2014)] can be observed on the orientation of the optimal planes and on the stress change resolved on these planes (King et al., 1994).

Considering the uncertainties with regard to the physical properties of the crust, particularly the geometry of the slip areas, ΔCFS can be estimated only within one order of magnitude. Based on these considerations, all values of ΔCFS, reported in Table 1, were calculated using values of 0.4 for effective friction and 80 GPa for Young's modulus, and values > 1 bar were rounded up to the nearest integer.

3. Co-seismic Coulomb stress changes

3.1. Effect of the 1714 Bhutan earthquake

The 1714 event most likely had a magnitude *Mw* 8.0 ± 0.5, affecting the MHT under at least the western half of Bhutan (Hetényi et al., 2016b), and ruptured the surface along the MFT (Berthet et al., 2014; Le Roux-Mallouf et al., 2016). We found that the 1714 slip on the MHT changed the Coulomb stress over the entire Bhutan Himalayas and its immediate foreland (Fig. 2a). The stress drop on the slipped patch was ~19 bar, which caused an increase in ΔCFS and clamping in an area ~30–40 km from the slipped patch (Fig. S3). ΔCFS on the DCF was larger than that on the Kopili strike-slip fault (Table 1, Fig. 3). The increase in ΔCFS and unclamping along the DCF below the depth of the MHT as well as the decrease in ΔCFS and clamping in the upper 10 km are reflected in the current seismicity (Fig. 3). Furthermore, ΔCFS on the faults bounding the Shillong Plateau was noted to be insignificant (Fig. 2c and d).

3.2. Effect of the 1897 Assam earthquake

The *Mw* 8.25 ± 0.1 earthquake occurred along the putative Oldham Fault (Bilham and England, 2001) that slipped along about 79 km, from > 5 km to 30–40 km depth with an average slip of 25 ± 5 m (England and Bilham, 2015). This is an unusual event according to empirical scaling between surface rupture length, width, slip, and the moment magnitude established using global data of large earthquakes (Wells and Coppersmith, 1994), but these are the only available data about slip and the rupture plane of the 1897 Assam earthquake. The earthquake caused stress changes that affected the entire Shillong Plateau and the Bhutan Himalayan foreland and foothills (Figs. 4 and S2).

The stress drop on the slipped patch was ~111 bar. We found that the slip on the Oldham Fault led to ΔCFS on the Dauki Fault of up to −150/+227 bar (Table 1). The upper and lower halves of the Dauki Fault underwent negative and positive ΔCFS, respectively; however, the entire surface underwent positive normal stress change (unclamping). The eastern segment of the Dauki Fault underwent stress changes only at its western margin, which had a much lower magnitude although still

Table 1
Interseismic Coulomb stress change (ΔCFS) rate, and seismic ΔCFS and normal stress change ($\Delta\sigma_n$) along receiver faults caused by three earthquakes: the 1897 earthquake along the Oldham Fault, the 1714 Bhutan earthquake along the MHT, and a *M* 7 earthquake on one of the strike-slip faults. All the values are in bar. Bold values are stress drops along the source faults. (1) Adopting the highest slip rate of 6.2 mm yr^{-1} suggested by Vernant et al. (2014) and a 50° dip for the fault yields a slip of 9.6 mm yr^{-1} along the fault. (2) Loading by Dauki east. (3) Current geodetic data indicate an ~17 mm yr^{-1} contraction rate along the MHT. Because the ramp is dipping north at ~15° (Coutand et al., 2014), we infer a slip rate of 18 mm yr^{-1} along the fault. (4) Loading by MHT ramp. (5) Mean interseismic ΔCFS rate on an MHT patch of 170 km by 50 km (see Fig. 2).

Fault	Slip rate [mm yr^{-1}]	Interseismic stress loading rate [bar yr^{-1}]		Assam 1897		Bhutan 1714		Strike slip M7	
				ΔCFS	$\Delta\sigma_n$	ΔCFS	$\Delta\sigma_n$	ΔCFS	$\Delta\sigma_n$
Oldham (2)	?	−0.004	Top	**−110.82**	**13.45**	< 0.06			
		−0.03	Bottom						
Dauki west	3			−74	−208				
				153	256				
Dauki east	9.6 (1)	0.03		0.1	−7.5				
				7.4	−0.3				
DCF	~1	0.004		0.38	−1.0	−19	−101	**−13.7**	**0**
				0.08	−0.04	19	98		
Kopili	~5	0.02		−0.76	−0.63	−0.27	−0.47	**−13.7**	**0**
				1.62	3.5	1.59	1.27		
MFT				−2.1	−0.17				
				0.1	3.3				
MHT ramp aseismic slip	18 (3)	−0.06		−0.22	−0.004	0.004	−1.17		
				0.01	0.033	−17.2	1.31		
MHT flat	(4)	0.05	North	0.002	−0.006	−141.4	−19.7	< −0.5	
		−0.001	South	0.3	0.001	−99.2	−26.6		
MHT flat	(4)	0.03	(5)			**−19**	**1.6**		
MHT flat	17		(5)						

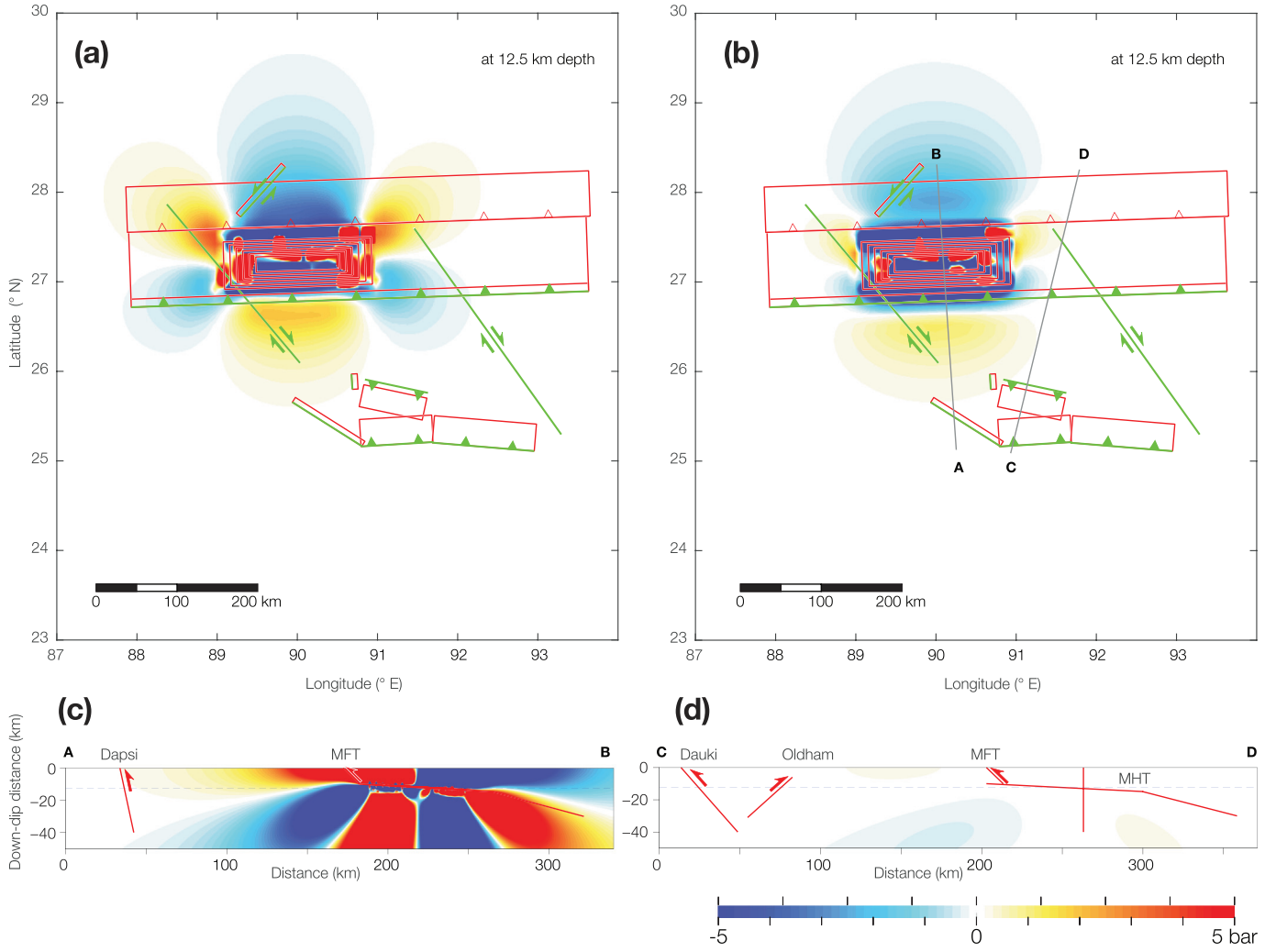

Fig. 2. Coulomb stress changes (ΔCFS) caused by the 1714 earthquake along the MHT in western Bhutan. An average slip of 7 m on the fault with the approximate slip area predicted by Hetényi et al. (2016b) (Fig. 1) yields M_W 8.3 (M_0 = 3.0E + 28 dyne cm), with a mean stress drop of ~19 bar. Linearly tapered slip is indicated by the six nested rectangles. Friction coefficient μ = 0.4, Young's modulus E = 80 GPa. (a) Map of ΔCFS along optimally oriented strike-slip faults. (b) Map of ΔCFS along optimally oriented reverse faults. Both maps are constructed for a depth of 12.5 km, which is the mean depth of the flat segment of the MHT in Bhutan. Cross sections (c) AB perpendicular to the strike of the MHT and MFT and (d) CD perpendicular to the strike of the Oldham Fault. Dashed lines on cross sections indicate the level of the map projection.

of several bars (Table 1, Fig. S4b).

The two strike-slip fault systems underwent disparate stress changes (Table 1); for both, the maximum change occurred along the central segment in the immediate foreland and beneath the sub-Himalayas (Figs. 3 and 4a). The MFT in western Bhutan underwent a ΔCFS of approximately −1 bar and a normal stress increase of approximately 2 bar in eastern Bhutan (Fig. 4). However, ΔCFS on the MHT was < 0.3 bar, with virtually no normal stress change (Fig. 4). The customary map of Coulomb stress change on optimally oriented thrust faults (Fig. 4b; e.g., Gahalaut et al., 2011) is therefore misleading, because the subhorizontal MHT is ~40° away from an optimal orientation.

3.3. DCF fault zone and the 1930 Dhubri earthquake

The *Mw* 7.1 Dhubri earthquake in 1930 (Gee, 1934), ANSS Comprehensive Earthquake Catalog, 2017) has been traditionally assigned to a NS-striking fault (Valdiya, 1976). As there is no geological evidence for such a fault, and according to the updated epicentre location (Fig. 1) by Szeliga et al. (2010), we simulated the earthquake along the southern end of the DCF (Diehl et al., 2017). Building on observations by Gee (1934), we assumed that the fault was blind (i.e., having maximum effect on the upper crustal stresses). Moreover, based on typical focal depths of the DCF, we assumed that the rupture was located at 15–30 km depth, where it would have only a small effect on the MHT, and < 10 km laterally from the intersection of the DCF and MHT. The effect of this rupture on the Shillong Plateau-bounding faults would have been even smaller, and the only significant effect would have been on the northern continuation of the DCF zone. Along the strike, the Coulomb stress increase would have affected the segment from the slipped part to beneath the Himalayan foothills (Fig. S5). The *Mw* 6.9 earthquake of 2011 in northern Sikkim (e.g., Paul et al., 2015) likely occurred along the same structure. In Figs. 3 and S5, we show the hypothetical scenario of a similar earthquake (Sutar et al., 2017) occurring in the Kopili Fault zone.

3.4. Interseismic stress loading rates

We compare co-seismic stress changes with the secular effect of interseismic strain accumulation to then estimate whether the return time of major events can be significantly altered by co-seismic Coulomb stress changes.

Current geodetic data indicate an ~17 mm yr^{-1} contraction rate

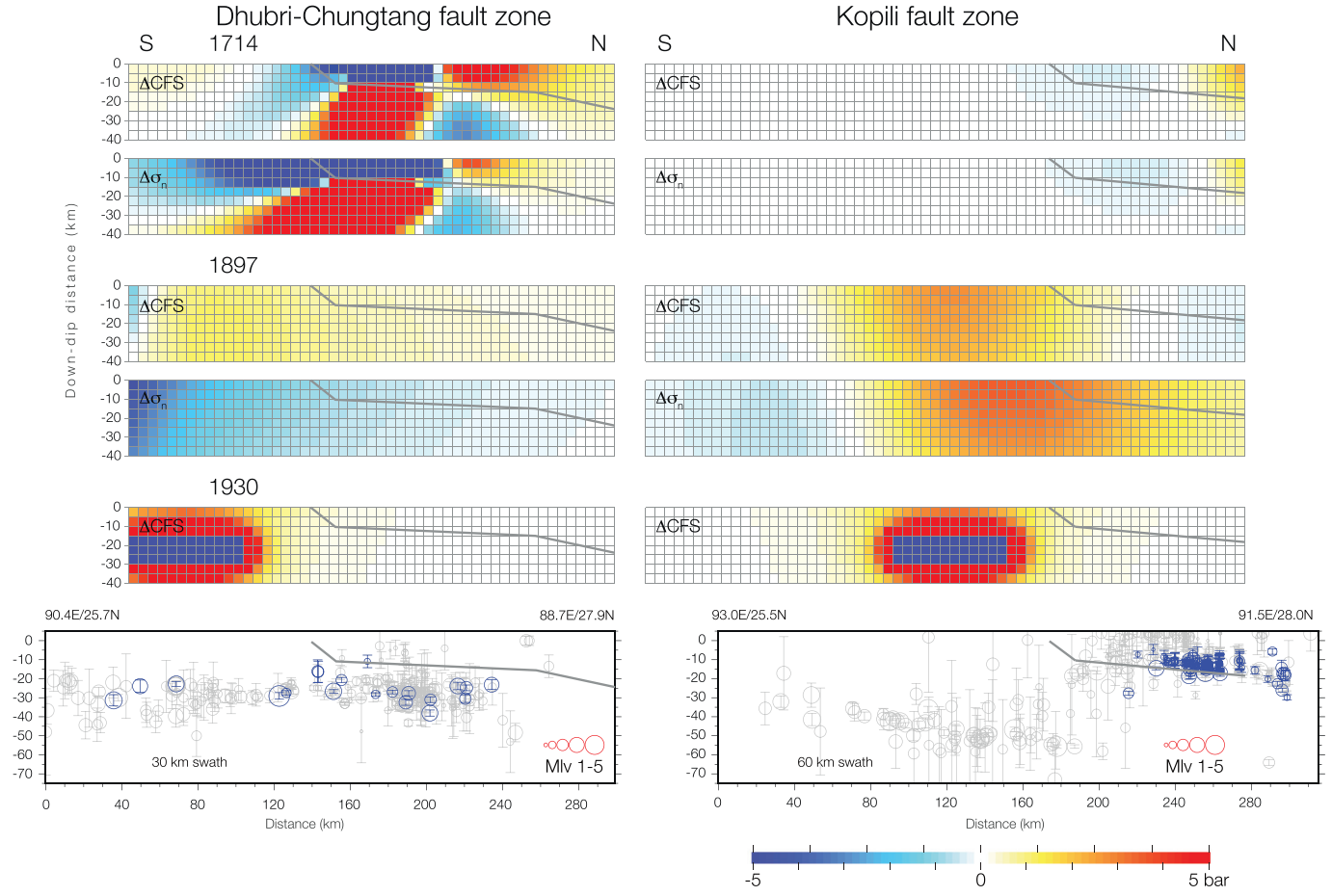

Fig. 3. Coulomb stress changes (ΔCFS) and normal stress changes ($\Delta\sigma_n$) resolved on the DCF and Kopili Fault zone planes in a rake direction of 180°. Three major historical earthquakes in the area are considered (see labels); the M_W 7.0 earthquake along the Kopili fault zone is hypothetical. Grid line spacing is 5 km. Thick grey line on all cross sections represents the MFT and MHT systems. Bottom panels show seismicity from the temporary GANSSER network (doi:10.12686/sed/networks/xa); grey symbols show all events, blue symbols show well-constrained events, and uncertainties represent location error in depth (see Diehl et al., 2017 for details).

along the MHT, and while its flat part in western Bhutan is locked (Marechal et al., 2016), diffuse seismic activity occurs on the MHT ramp (Diehl et al., 2017; Singer et al., 2017), as shown in Fig. 3. Accordingly, the steady aseismic slip, along the MHT ramp, or creep along its deep ductile part, yields an interseismic ΔCFS rate of approximately -0.06 bar yr^{-1}, which results in the interseismic ΔCFS rate along the MHT flat to decrease from the internal to the proximal parts (Fig. S6). For comparison, the mean interseismic ΔCFS rate on an MHT patch of 170 km by 50 km (equivalent to the estimated rupture area of the 1714 earthquake) is ~0.03 bar yr^{-1}.

The slip rates across the faults around the Shillong Plateau are less well constrained. According to available data, the highest slip rates occur along the Dauki Fault (Table 1), but the values vary greatly among past studies and along the strike (Banerjee et al., 2008; Bilham and England, 2001; Biswas et al., 2007; Clark and Bilham, 2008; Vernant et al., 2014; Barman et al., 2016). Even when considering the highest slip rates, the stress loading rate along the Dauki Fault is on the order of 10^{-2} bar yr^{-1}, and the GPS slip rates are nil within the error along the Oldham Fault (Fig. 6; Barman et al., 2016). Furthermore, hypothetical interseismic loading along the Oldham Fault caused by apparently aseismic slip along the Dauki Fault would be positive in the lower eastern corner and negative in the upper western half of the Oldham Fault (Fig. S7). This indicates that the currently accepted geometry of the Oldham and Dauki faults at depth is incorrect and requires an understanding of the source of the stresses that caused the 1897 Assam earthquake. Additionally, there is no evidence for a geologically significant displacement along the Oldham Fault (Biswas et al., 2007; Rosenkranz et al., 2018), suggesting that the backthrust was activated only recently.

The shape of buried folds in the sediments of the Sylhet trough to the south of the Shillong Plateau (blue axial traces in Fig. 1) indicates that there is coeval E–W and N–S shortening. Additionally, the onset of thickening of the sediments toward the Dauki Fault at about 3.5–2 Ma suggests an increase in sediment accumulation rates, basin subsidence rates, and/or fault slip rates at 3.5 to ~2 Ma (Najman et al., 2016).

4. Discussion

4.1. Did the 1897 Assam earthquake form a stress shadow in the eastern Himalaya?

The apparent low seismicity in the Bhutan Himalayas (Bilham and England, 2001; Gahalaut et al., 2011) was not caused by a reduction in the Coulomb stresses (i.e., stress shadow) due to the 1897 Assam earthquake. The misinterpretation of stress transfer by Gahalaut et al. (2011) stems from their assumption that the ΔCFS field for optimally oriented thrust faults should be used (e.g., Fig. 4b in this study), which they did to infer ΔCFS along the MHT. While the assumption is applicable to the MFT (Fig. 5b), it cannot be applied to the MHT, as ΔCFS along the sub-horizontal MHT is positive (Fig. 5a). Furthermore, a coseismic stress loading of 0.1–0.2 bar from an Oldham Fault M 8 earthquake on the MHT in eastern Bhutan would advance the time to the next MHT M 8 earthquake in the region by 3–7 years, because the interseismic stress loading rate on the MHT in Bhutan is on the order of

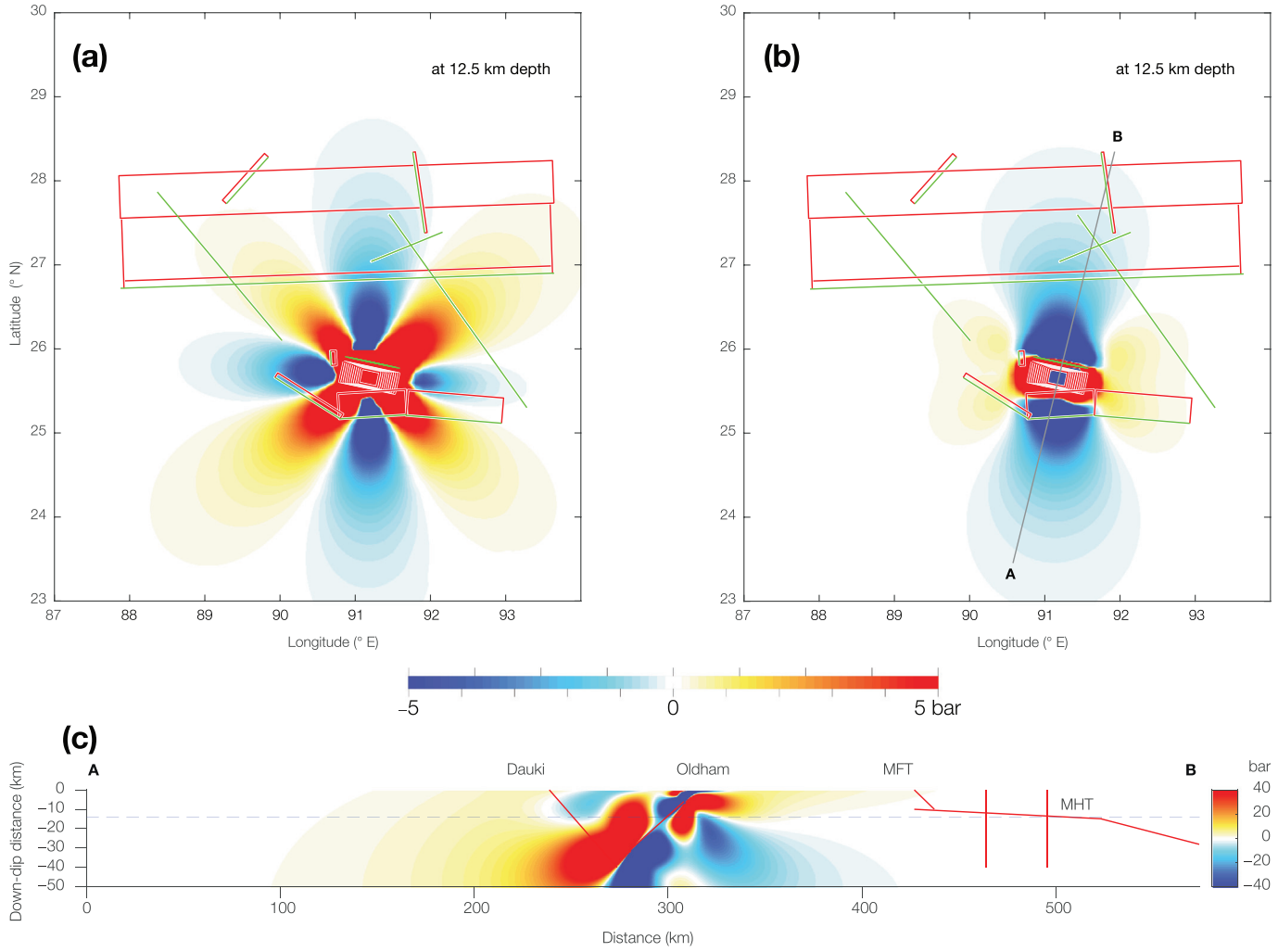

Fig. 4. Coulomb stress changes (ΔCFS) caused by the 1897 earthquake around the Shillong Plateau and along the Oldham Fault. Calculations are for μ = 0.4 and E = 80 GPa. Map of ΔCFS for (a) optimally oriented strike-slip faults and (b) optimally oriented thrust faults constructed for a depth of 12.5 km, which is the mean depth of the flat segment of the MHT in Bhutan (#11 in Fig. S1). (c) Cross section AB perpendicular to the strike of the MFT showing stresses acting on nearby optimally oriented thrust faults. Note the large (> 200 bar) ΔCFS value at the lower half of the Dauki Fault (#2 in Fig. S1) and the apparent negative ΔCFS value on the MHT. See related text and Fig. 5 regarding the resolved Coulomb stress along the MHT.

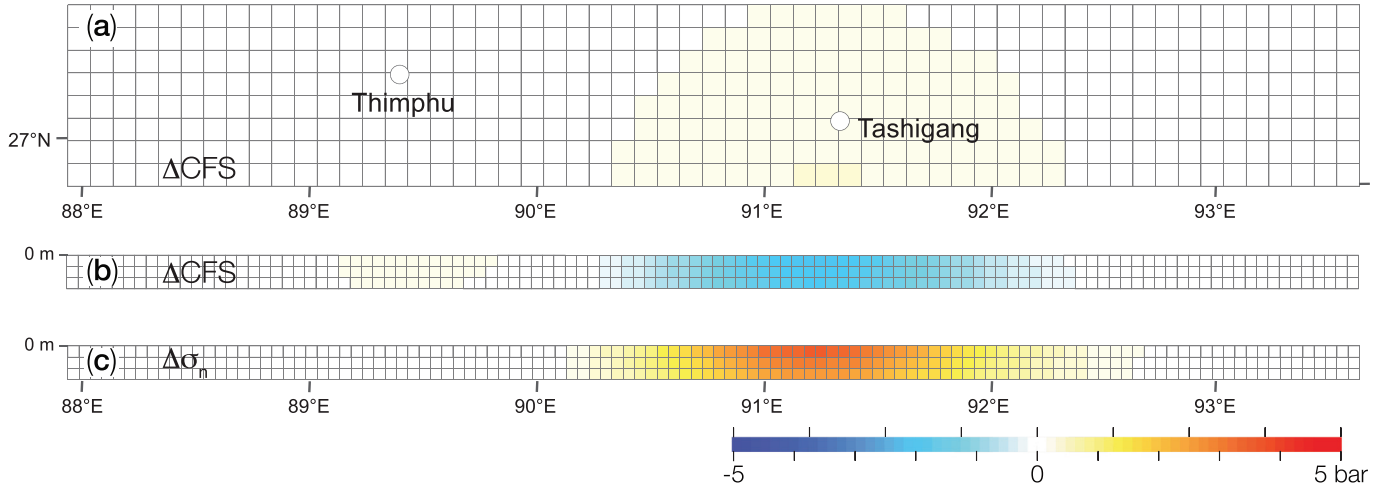

Fig. 5. Coulomb stress changes (ΔCFS) after the 1897 earthquake resolved on the (a) MHT and (b) MFT in a rake direction of 90°. (c) Normal stress change ($\Delta\sigma_n$) along the MFT. Grid line spacing is 5 km along the MFT and 10 km along the MHT. See related text and Fig. 4 regarding ΔCFS caused by the 1897 earthquake along the Oldham Fault.

$\sim$0.03 bar yr^{-1}. Hence, this variation is apparently insignificant because the return times of great and large earthquakes in eastern Nepal probably ranged between 750 ± 140 and 870 ± 350 years (Bollinger et al., 2014).

On the other hand, a major seismic event along the Oldham Fault would transfer Coulomb stresses to the strike-slip fault systems, indirectly affecting the Himalayan faults. The transfer of stresses to the Kopili system is more significant because of the larger Coulomb stresses and positive normal stresses, while the Coulomb stresses on the DCF are one order of magnitude smaller and the normal stresses are negative (clamping). Equivalent ΔCFS along the strike-slip fault zones would be caused by an M_W 8 event along the Dauki fault (Figs. S8 and S9). ΔCFS along the Kopili Fault in the foreland of the eastern Bhutan Himalayas would be $\sim$1.1 bar in a patch that is 60 km long and 15 km wide and would likely trigger M 7 strike-slip earthquakes to the south of the MFT. Conversely, an M 7 rupture along these strike-slip faults would increase the stresses by 0.35 bar along an MHT patch that is 170 km long and 50 km wide, advancing the time to the next earthquake along the MHT by a dozen years. Consequently, ruptures along the Shillong Plateau-bounding fault system could indirectly affect eastern Bhutan more than western Bhutan.

Over geological timescales, stress interaction between the Oldham Fault and the Himalayan faults may therefore be significant, because large earthquakes along the former always affect the eastern Bhutan Himalayas more than the western Bhutan Himalayas, which would lead to long-term lateral variations in interseismic coupling along the MHT between western and eastern Bhutan. These stress transfers may have been occurring since 9–15 Ma when the reverse slip along the Dauki Fault initiated (Biswas et al., 2007; Clark and Bilham, 2008).

4.2. Effect of major Bhutan earthquakes on faults bounding the Shillong Plateau

The hypothesis of a jump of the Himalayan orogenic front from the MFT to the Dauki Fault implies that the two strike-slip systems are transform faults. However, the strike-slip seismicity in the Himalayas is beneath the MHT and the strike-slip faults do not offset the MFT or any other Himalayan structure. Notwithstanding, a Himalayan M 8 earthquake could trigger slip along these strike-slip faults. For the 1714 Bhutan earthquake, about 25% of the adjacent 40-km-wide patch of the MHT experienced ΔCFS > 1 bar. Therefore, if a transverse strike-slip fault is more than $\sim$40 km away from the rupture surface, ΔCFS on it will be $\ll$1 bar. However, if the rupture along the MHT overlaps a strike-slip fault, ΔCFS would be $\sim$0.9 bar in a patch that is 60 km long and 15 km wide and would likely trigger or significantly advance M 7 strike-slip earthquakes beneath the MHT. In contrast, even if an M 7 earthquake occurred along the southern ends of the strike-slip faults, it would not transfer stresses to the faults bounding the Shillong Plateau. Therefore, major seismic events along the MHT (even if it was blind) do not cause significant Coulomb stress changes in the Shillong Plateau, neither directly nor indirectly (via transfer faults). This is due to a nonoptimal orientation of the respective receiver faults.

We assume that the postseismic creep along the MHT would have no significant effect on stress transfer between the fault systems. For example, postseismic deformation from GPS and InSAR measurements over two years after the Mw 7.8 Gorkha event is mostly related to afterslip at the downdip end of the rupture, with a maximum afterslip of $\sim$0.3 m (Wang and Fialko, 2017). Hence, in this specific case postseismic relaxation did not cause slip on the shallow part of the MFT.

4.3. Stress loading along the Oldham fault

The close Oldham and Dauki faults are an apparently cross-cutting set of faults, they have nearly optimal stress orientations, and a slip on one would cause increase in ΔCFS and unclamping along the other; therefore, they are in an instantaneous dynamical triggering setup (*sec.*, Fan and Shearer, 2016). Tectonic loading across the Dauki Fault, assuming steady slip and a mean estimated stress loading rate of 0.02 bar a^{-1}, would cause Coulomb stress loading on the Oldham Fault at the level of stress drop as that caused by the 1897 earthquake (approximately $-$73 bar) over a timescale of $\sim$3600 years. This value is in agreement with that obtained from a simple calculation of dividing the average slip of 25 m during the 1897 earthquake (England and Bilham, 2015) by the mean slip rate of 5 mm a^{-1}, resulting in a recurrence time of 5000 years; the value is also in agreement with the estimate of 3000–8000 years by Bilham and England (2001). Evidence for a much shorter recurrence interval of $\sim$500 years (Sukhija et al., 1999) could just as well be evidence for the recurrence scale of large earthquakes along the DCF zone because of the proximity of the investigated sites and lack of structural context. The problem with our estimates is that only one quarter of the Oldham Fault undergoes stress increase by interseismic stress loading transferred from the Dauki Fault, while the rest undergoes Coulomb stress decrease; even when averaged over the entire surface, the Coulomb stress change is negative. These values are, however, underestimated because we investigated stress transfer only from the neighbouring faults and omitted postseismic downdip creep and asthenospheric relaxation. Additionally, the N-S component of the GPS velocities does not change across the putative trace of the Oldham fault (Vernant et al., 2014; Barman et al., 2016; Table S1), suggesting that the current contraction across the fault is nil within the resolution of the published GPS data, and that the fault may be locked.

4.4. Existence of a new or diffuse plate boundary

The shortening in the northeastern margin of the Indian Plate and the eastern Himalayas is accommodated within a broad deformation zone that can be described as a diffuse plate boundary (Thatcher, 1995), the width of which is influenced by the character of the intraplate boundary and the size of which controls the resistive forces exerted upon the subducting plate (Copley et al., 2010). Within diffuse plate boundaries, deformation is distributed across wider regions and accommodated by several fault systems with variable slip rates (Bennett et al., 2003; Thatcher, 1995). Consequently, earthquakes within diffuse plate boundaries occur in spatially and temporally complex patterns. Although previous studies and this study agree that the northeastern corner of the Indian Plate is being fragmented (Clark and Bilham, 2008; Vernant et al., 2014), with the least deforming part of this area being the Shillong Plateau (see Fig. 6), the causative relationships between the active structures within the Indian Plate and in the Himalaya–Tibet orogen remain unclear due to insufficient information at depth.

Deformation in the foreland of the eastern Himalayas may be part of the continent-scale initiation of tectonic activity since 15 Ma along the margins of the Tibetan Plateau (Molnar and Stock, 2009). Removal of mantle lithosphere from beneath Tibet, or from part of it, would lead to a change in the balance of forces per unit length applied to the Indian and Eurasian plates (Molnar and Stock, 2009). Variations in crustal structure in Bhutan, proposed to be driven by the presence (absence) of an Indian mantle-slab to the northwest (northeast) of Bhutan (Singer et al., 2017), may contribute to this scenario.

Alternatively, the dismemberment of the northeastern corner of the Indian Plate may be caused by the change in regional stress applied along the India–Eurasia–Burma plate boundaries (Clark and Bilham, 2008). The collisional boundary in the eastern Himalayan system may be poorly coupled due to introduction of dense oceanic and/or transitional crust into the eastern plate margin (Clark and Bilham, 2008). This transition is marked by a “hinge zone” (Fig. 7), which divides the onshore part of the Bengal Basin into a platform or shelf slope to the west and northwest and a basinal facies, the Bengal foredeep to the south (Alam et al., 2003; Salt et al., 1986). The basement of the Indian Plate underlies the shelf, while the deeper basin to the east and south may be floored by oceanic or transitional crust (Sibuet et al., 2016; Talwani et al., 2016, respectively). The Dauki Fault truncates the hinge

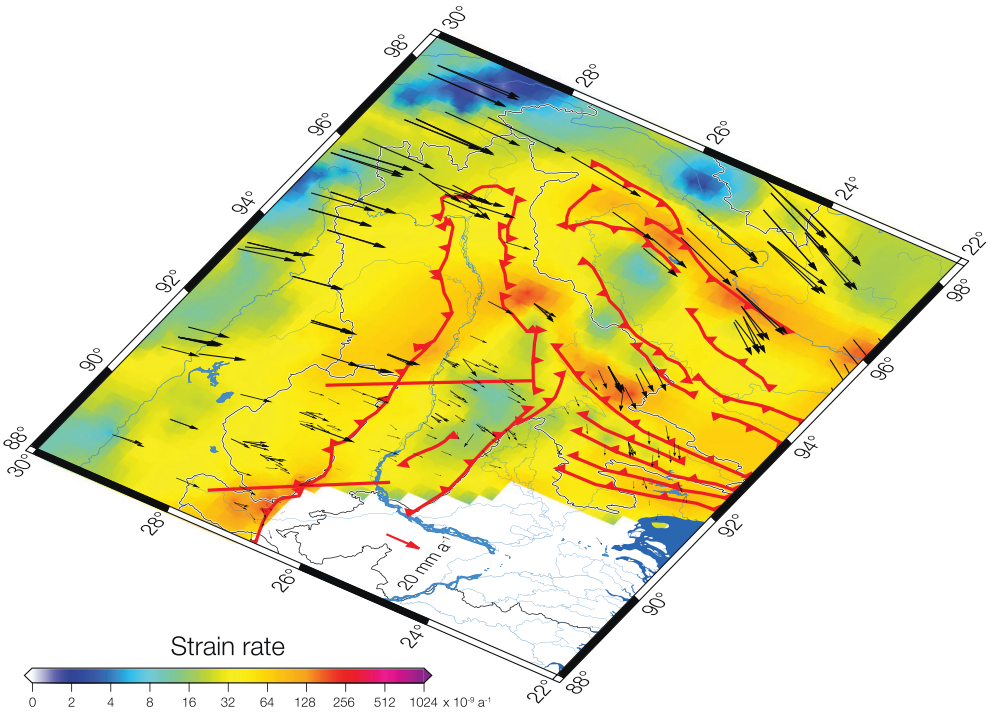

Fig. 6. Strain rate map from Kreemer et al. (2014); scale units are $10^{-9}\,a^{-1}$. Black arrows: GPS velocity vectors with respect to India fixed from Gahalaut et al. (2011), Vernant et al. (2014) Marechal et al. (2016) and Steckler et al. (2016). The red, southward-pointing arrow in the mid-west is the 20 mm yr^{-1} scale. Traces of thrust faults have been taken from Styron et al. (2010). In this view, the Shillong Plateau seems to be pinched between two orogens.

zone (Fig. 7), and therefore, it may thrust continental crust of normal thickness over an oceanic or transitional crust covered by at least 10 km of Cenozoic platform sediments. The same, supposedly Cretaceous, oceanic crust is being subducted to the east beneath the Indo-Burman Ranges (e.g., Steckler et al., 2016), which are the surface expression of a wide forearc and accretionary prism. The highly oblique convergence between the Indian Plate beneath the Shan Plateau (eastern Burma) at 46 mm yr^{-1} is partitioned into a 42 mm yr^{-1} dextral slip across several NS-trending strike-slip faults and an ~18 mm yr^{-1} convergence (Steckler et al., 2016). These southwestward-directed velocities of the Indo-Burman Ranges provide apparent dextral kinematics to the Dauki Fault (Fig. 6). The difference in crustal thickness and the bending stresses from the Indo-Burman Ranges in the east and Bengal fan sediments to the south might have led to a failure of the crustal transition located currently beneath the southern edge of the Shillong Plateau and activation of the Dauki Fault at 9–15 Ma (Biswas et al., 2007; Clark and Bilham, 2008). This process is therefore different from the Himalayan processes and may not represent a southward jump of the orogen (Vernant et al., 2014).

The 3–6 mm yr^{-1} contraction rate across the Dauki Fault apparently does not reduce the contraction rates in the Bhutan Himalayas in its lee, because the contraction rates in this area are same as those in the Nepal Himalayas (Marechal et al., 2016). The slip along the Dauki Fault may simply be caused by a faster northward movement of the basement of the Bengal Basin, as suggested by the GPS vectors in the Surma Basin that are more NS-oriented compared with the oblique vectors toward the east (Fig. 6). This movement may be aided or caused by oblique subduction of the Indian plate beneath the Burma arc, and related slab pull toward the NNE and slab bending toward the east and north beneath the two converging orogenic wedges pinching the Shillong block between them and deforming the Surma Basin sediments into two orthogonal sets of folds (Fig. 7). The Dauki Fault is at the site of a former mid-ocean spreading ridge (M0, 120 Ma; Talwani et al., 2016), suggesting that the Dauki Fault is a weak crustal zone in which the fault was reactivated as a thrust in middle Miocene. Therefore, this fault may be a component within a diffuse plate boundary, rather than that marking the jump of the Himalayan orogenic front into its foreland. Consequently, the great Assam earthquake of 1897 (*Mw* ~8.25) may not have been an intraplate earthquake.

If the crust beneath the Bengal Basin is still attached to the Indian crust to the west, the difference in thrusting rate over thin vs. normal continental crust in the east and west, respectively, is accommodated by the dextral movement along the NW-trending DCF and Kopili Fault zones. Seismicity along the DCF system is present beneath the MHT (Diehl et al., 2017; Fig. 3), which may also be the case for the Kopili fault system. Therefore, the MHT decouples the deformation in the Himalayan wedge from the seismogenic basement. Furthermore, the DCF and Kopili Fault are mostly related to the segmentation of the Indian Plate and not of the Himalayan wedge. Along these two diffuse boundaries, the Shillong block, driven by the weak Dauki Fault, is detaching from the Indian Plate, the northward motion of which is resisted by the active Himalayan orogenic wedge.

5. Conclusions

Calculations of Coulomb stress transfer between several source and receiver faults in the Bhutan–Shillong system suggest the following:

1. The Bhutan Himalaya and Shillong Plateau stress regimes are less connected than previously suggested.
2. Slip on the thrusts in the Bhutan Himalaya does not produce a significant stress shadow on the faults bounding the Shillong Plateau, and vice versa.
3. The state of stress in Bhutan is influenced (to a very small extent) by seismic stress transfer from both the Oldham Fault and the Kopili Fault. Deformation within the Shillong Plateau affects more the deformation within the eastern Bhutan Himalayas in the lee of the plateau.
4. Western and eastern Bhutan seem to have different interseismic loading patterns; therefore, they may follow different seismic cycles and produce major earthquakes with different characteristics.
5. Because the MHT, MFT (at least since 2 Ma), and Dauki Fault have been coevally active over geologic time periods (since 9–15 Ma), a minor influence of the Shillong faults on the eastern Bhutan faults may contribute to the observed along-strike differences in current seismicity and interseismic coupling.

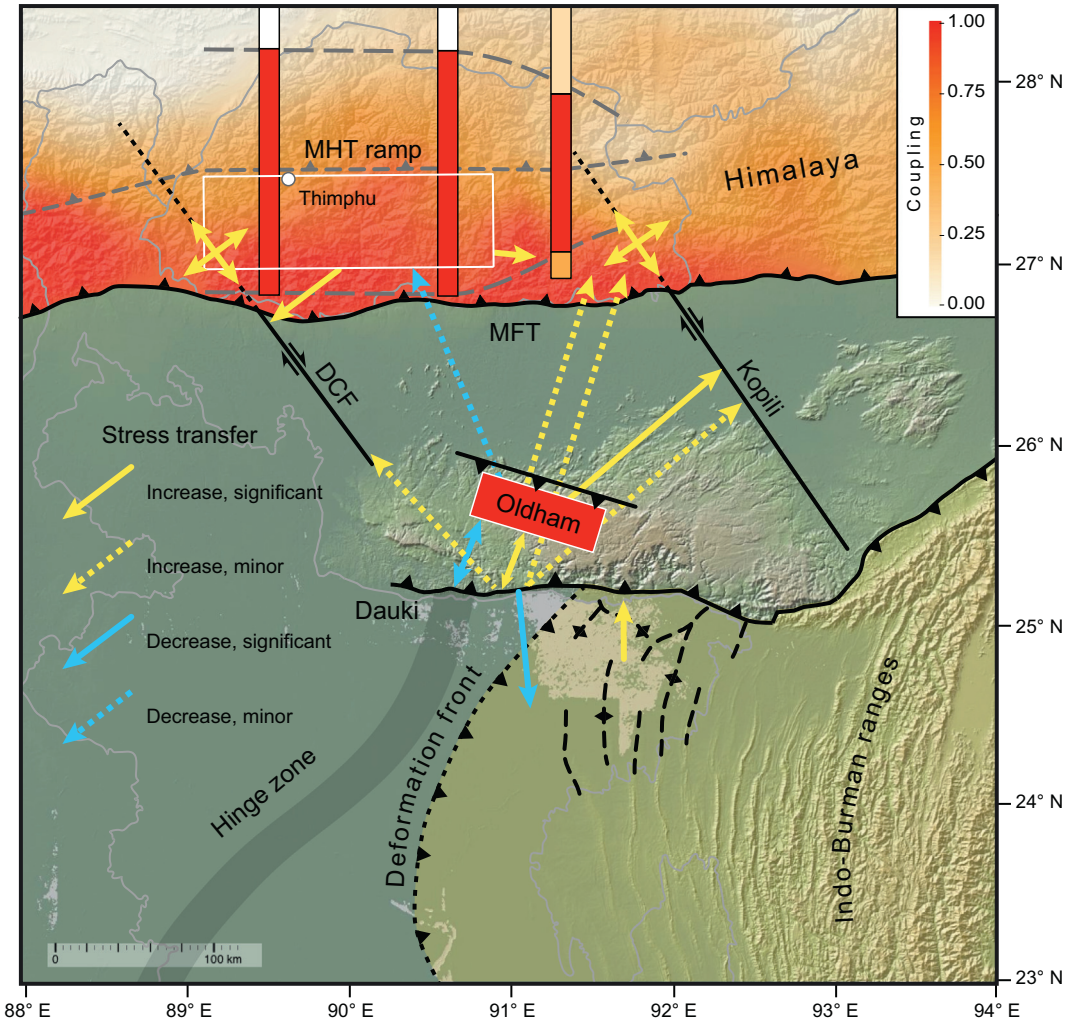

Fig. 7. Schematic diagram of co-seismic ΔCFS transfer directions in the Bhutan–Shillong plateau system. Orange arrow: Coulomb stress increase. Pale blue arrow: Coulomb stress decrease. Arrows start at the source faults and end at the receiver faults. Dashed arrows: minor ΔCFS transfer, thick arrows major ΔCFS transfer. Blue patch in the eastern Bhutan Himalayas is the presumed hypocentre of the 1714 earthquake along the MHT (Hetényi et al., 2016b), estimated to be currently fully locked (Marechal et al., 2016). The MHT flat in the eastern Bhutan Himalayas is currently a seismic and partially creeping segment of the MHT (Marechal et al., 2016). The colored base map represents the estimates of interseismic coupling of the Main Himalayan Thrust by Stevens and Avouac (2015). The red rectangle over the Shillong Plateau represents the estimated rupture area of the 1897 Assam earthquake (England and Bilham, 2015). Structures in purple are Himalayan, and structures in red primarily affect the Indian crust. Structures in blue are related to the Indo-Burman Ranges; their eastern boundary is a blind thrust—the deformation front by Steckler et al. (2016). The Indian crust to the east of the "hinge zone" is a thinned transitional crust or oceanic crust.

6. The tectonics of the Shillong Plateau is governed by the change in crustal character to its south and by its highly oblique subduction to the northeast, and to a lesser extent, by the Himalayan tectonics.

Acknowledgments

DG thanks the Herbette Foundation and the Swiss National Science Foundation for financial support (visiting professorship grants, SNSF grant number IZK0Z2_167848) during the preparation of the manuscript at the University of Lausanne. This project is partly supported by project OROG3NY (Swiss National Science Foundation, grant PP00P2_157627) and the French Agence Nationale de la Recherche (ANR-13-BS06-0006-01). Critical comments by M Delescluse, J Hubbard, and L Seeber are greatly acknowledged.

Appendix A. Supplementary data

Supplementary data to this article can be found online at https://doi.org/10.1016/j.tecto.2018.07.018.

References

Alam, M., Alam, M.M., Curray, J.R., Chowdhury, M.L.R., Gani, M.R., 2003. An overview of the sedimentary geology of the Bengal Basin in relation to the regional tectonic framework and basin-fill history. Sediment. Geol. 155, 179–208.

ANSS Comprehensive Earthquake Catalog (ComCat), December 09, 2017. https://earthquake.usgs.gov/earthquakes/eventpage/iscgem907472#executive.

Banerjee, P., Bürgmann, R., Nagarajan, B., Apel, E., 2008. Intraplate deformation of the Indian subcontinent. Geophys. Res. Lett. 35. https://doi.org/10.1029/2008GL035468.

Barman, P., Jade, S., Shrungeshwara, T., Kumar, A., Bhattacharyya, S., Ray, J.D., Jagannathan, S., Jamir, W.M., 2016. Crustal deformation rates in Assam Valley, Shillong Plateau, Eastern Himalaya, and Indo-Burmese region from 11 years (2002 – 2013) of GPS measurements. Int. J. Earth Sci. 1–14.

Bennett, R., Wernicke, B., Niemi, N., Friedrich, A., Davis, J., 2003. Contemporary strain rates in the northern Basin and Range province from GPS data. Tectonics 22, 1008.

Berthet, T., Hetényi, G., Cattin, R., Sapkota, S.N., Champollion, C., Kandel, T., Doerflinger, E., Drukpa, D., Lechmann, S., Bonnin, M., 2013. Lateral uniformity of India Plate strength over central and eastern Nepal. Geophys. J. Int. 195, 1481–1493.

Berthet, T., Ritz, J.-F., Ferry, M., Pelgay, P., Cattin, R., Drukpa, D., Braucher, R., Hetényi, G., 2014. Active tectonics of the eastern Himalaya: new constraints from the first tectonic geomorphology study in southern Bhutan. Geology 42, 427–430.

Bilham, R., England, P., 2001. Plateau 'pop-up' in the great 1897 Assam earthquake. Nature 410, 806–809.

Biswas, S., Coutand, I., Grujic, D., Hager, C., Stöckli, D., Grasemann, B., 2007.

Exhumation and uplift of the Shillong plateau and its influence on the eastern Himalayas: new constraints from apatite and zircon (U-Th-[Sm])/He and apatite fission track analyses. Tectonics 26 (n/a-n/a).
Bollinger, L., Sapkota, S.N., Tapponnier, P., Klinger, Y., Rizza, M., Van Der Woerd, J., Tiwari, D., Pandey, R., Bitri, A., Bes de Berc, S., 2014. Estimating the return times of great Himalayan earthquakes in eastern Nepal: evidence from the Patu and Bardibas strands of the Main Frontal Thrust. J. Geophys. Res. Solid Earth 119, 7123–7163.
Cattin, R., Avouac, J., 2000. Modeling mountain building and the seismic cycle in the Himalaya of Nepal. J. Geophys. Res. 105, 13,389–313,407.
Clark, M.K., Bilham, R., 2008. Miocene rise of the Shillong Plateau and the beginning of the end for the Eastern Himalaya. Earth Planet. Sci. Lett. 269, 337–351.
Copley, A., Avouac, J.-P., Royer, J.-Y., 2010. India-Asia collision and the Cenozoic slowdown of the Indian plate: implications for the forces driving plate motions. J. Geophys. Res. 115, B03410.
Coutand, I., Whipp, D.M., Grujic, D., Bernet, M., Fellin, M.G., Bookhagen, B., Landry, K.R., Ghalley, S., Duncan, C., 2014. Geometry and kinematics of the Main Himalayan Thrust and Neogene crustal exhumation in the Bhutanese Himalaya derived from inversion of multithermochronologic data. J. Geophys. Res. Solid Earth 119, 1446–1481.
Diehl, T., Singer, J., Hetényi, G., Grujic, D., Clinton, J., Giardini, D., Kissling, E., Group, G.W, 2017. Seismotectonics of Bhutan: evidence for segmentation of the Eastern Himalayas and link to foreland deformation. Earth Planet. Sci. Lett. 471, 54–64.
Drukpa, D., Velasco, A.A., Doser, D.I., 2006. Seismicity in the Kingdom of Bhutan (1937–2003): evidence for crustal transcurrent deformation. J. Geophys. Res. 111. https://doi.org/10.1029/2004JB003087.
England, P., Bilham, R., 2015. The Shillong Plateau and the great 1897 Assam earthquake. Tectonics 34, 1792–1812.
Fan, W., Shearer, P.M., 2016. Local near instantaneously dynamically triggered aftershocks of large earthquakes. Science 353 (6304), 1133–1136.
Gahalaut, V., Rajput, S., Kundu, B., 2011. Low seismicity in the Bhutan Himalaya and the stress shadow of the 1897 Shillong Plateau earthquake. Phys. Earth Planet. Inter. 186, 97–102.
Gansser, A., 1983. Geology of the Bhutan Himalaya. 181. Birkhäuser Verlag, Denkschriften der Schweizerischen Naturforschenden Geselschaft, Basel-Boston-Stuttgart, pp. 188.
Gee, E.R., 1934. The Dhubri Earthquake of the 3rd July, 1930. Mem. Geol. Surv. India 65, 1–106.
Hammer, P., Berthet, T., Hetényi, G., Cattin, R., Drukpa, D., Chophel, J., Lechmann, S., Moigne, N.L., Champollion, C., Doerflinger, E., 2013. Flexure of the India plate underneath the Bhutan Himalaya. Geophys. Res. Lett. 40, 4225–4230.
Hetényi, G., Cattin, R., Berthet, T., Le Moigne, N., Chophel, J., Lechmann, S., Hammer, P., Drukpa, D., Sapkota, S.N., Gautier, S., 2016a. Segmentation of the Himalayas as revealed by arc-parallel gravity anomalies. Sci. Rep. 6.
Hetényi, G., Le Roux-Mallouf, R., Berthet, T., Cattin, R., Cauzzi, C., Phuntsho, K., Grolimund, R., 2016b. Joint approach combining damage and paleoseismology observations constrains the 1714 AD Bhutan earthquake at magnitude 8 ± 0.5. Geophys. Res. Lett. 43.
Jaquet, Y., Duretz, T., Grujic, D., Masson, H., Schmalholz, S.M., 2017. Formation of orogenic wedges and crustal shear zones by thermal softening, associated topographic evolution and application to natural orogens. Tectonophysics. https://doi.org/10.1016/j.tecto.2017.07.021.
King, G.C.P., Stein, R.S., Lin, J., 1994. Static stress changes and the triggering of earthquakes. Bull. Seismol. Soc. Am. 84, 935–953.
Kreemer, C., Blewitt, G., Klein, E.C., 2014. A geodetic plate motion and global strain rate model. Geochem. Geophys. Geosyst. 15.
Kumar, A., Mitra, S., Suresh, G., 2015. Seismotectonics of the eastern Himalayan and Indo-Burman plate boundary systems. Tectonics 34, 2279–2295.
Le Roux-Mallouf, R., Ferry, M., Ritz, J.F., Berthet, T., Cattin, R., Drukpa, D., 2016. First paleoseismic evidence for great surface-rupturing earthquakes in the Bhutan Himalayas. J. Geophys. Res. Solid Earth 121, 7271–7283.
Lin, J., Stein, R.S., 2004. Stress triggering in thrust and subduction earthquakes and stress interaction between the southern San Andreas and nearby thrust and strike-slip faults. J. Geophys. Res. Solid Earth 109.
Long, S., McQuarrie, N., Tobgay, T., Grujic, D., Hollister, L., 2011. Geologic map of Bhutan. J. Maps 7, 184–192.
Ma, K.F., Chan, C.H., Stein, R.S., 2005. Response of seismicity to Coulomb stress triggers and shadows of the 1999 Mw = 7.6 Chi-Chi, Taiwan, earthquake. J. Geophys. Res. Solid Earth 110.
Marechal, A., Mazzotti, S., Cattin, R., Cazes, G., Vernant, P., Drukpa, D., Thinley, K., Tarayoun, A., Le Roux-Mallouf, R., Thapa, B.B., Pelgay, P., Gyeltshen, J., Doerflinger, E., Gautier, S., 2016. Evidence of interseismic coupling variations along the Bhutan Himalayan arc from new GPS data. Geophys. Res. Lett. 43, 12,399–312,406.
Molnar, P., 1987. The distribution of intensity associated with the great 1897 Assam earthquake and bounds on the extent of the rupture zone. J. Geol. Soc. India 30, 13–27.
Molnar, P., Pandey, M., 1989. Earth and Planetary Science. Proceedings of the Indian Academy of Sciences-Earth and Planetary Sciences 98. pp. 61–70.
Molnar, P., Stock, J.M., 2009. Slowing of India's convergence with Eurasia since 20 Ma and its implications for Tibetan mantle dynamics. Tectonics 28 (n/a-n/a).
Morino, M., Kamal, A.M., Muslim, D., Ali, R.M.E., Kamal, M.A., Rahman, M.Z., Kaneko, F., 2011. Seismic event of the Dauki Fault in 16th century confirmed by trench investigation at Gabrakhari Village, Haluaghat, Mymensingh, Bangladesh. J. Asian Earth Sci. 42, 492–498.
Najman, Y., Bracciali, L., Parrish, R.R., Chisty, E., Copley, A., 2016. Evolving strain partitioning in the Eastern Himalaya: the growth of the Shillong Plateau. Earth Planet. Sci. Lett. 433, 1–9.
Oldham, R.D., 1899. Report of the great earthquake of 12th June 1897. Mem. Geol. Surv. India 29, 1–379.
Paul, H., Mitra, S., Bhattacharya, S., Suresh, G., 2015. Active transverse faulting within underthrust Indian crust beneath the Sikkim Himalaya. Geophys. J. Int. 201, 1072–1083.
Rajendran, C., Rajendran, K., Duarah, B., Baruah, S., Earnest, A., 2004. Interpreting the style of faulting and paleoseismicity associated with the 1897 Shillong, northeast India, earthquake: implications for regional tectonism. Tectonics 23.
Rosenkranz, R., Schildgen, T., Wittmann, H., Spiegel, C., 2018. Coupling erosion and topographic development in the rainiest place on Earth: reconstructing the Shillong Plateau uplift history with in-situ cosmogenic ^{10}Be. Earth Planet. Sci. Lett. 483, 39–51.
Salt, C., Alam, M.M., Hossain, M.M., 1986. Bengal Basin: current exploration of the Hinge Zone Area of South-western Bangladesh. In: Proceedings of the South East Asia Petroleum Exploration Society VII, pp. 49–69.
Seeber, L., Armbruster, J.G., 1981. Great detachment earthquakes along the Himalayan arc and long-term forecasting. Earthquake prediction: an international review 4, 259–277.
Sibuet, J.-C., Klingelhoefer, F., Huang, Y.-P., Yeh, Y.-C., Rangin, C., Lee, C.-S., Hsu, S.-K., 2016. Thinned continental crust intruded by volcanics beneath the northern Bay of Bengal. Mar. Pet. Geol. 77, 471–486.
Singer, J., Kissling, E., Diehl, T., Hetényi, G., 2017. The underthrusting Indian crust and its role in collision dynamics of the Eastern Himalaya in Bhutan: insights from receiver function imaging. J. Geophys. Res. Solid Earth 122, 1152–1178.
Steckler, M.S., Mondal, D.R., Akhter, S.H., Seeber, L., Feng, L., Gale, J., Hill, E.M., Howe, M., 2016. Locked and loading megathrust linked to active subduction beneath the Indo-Burman Ranges. Nat. Geosci. 9, 615–618.
Stevens, V.L., Avouac, J.P., 2015. Interseismic coupling on the main Himalayan thrust. Geophys. Res. Lett. 42, 5828–5837. https://doi.org/10.1002/2015GL064845.
Styron, R., Taylor, M., Okoronkwo, K., 2010. Database of active structures from the Indo-Asian collision. EOS Trans. Am. Geophys. Union 91, 181–182.
Sukhija, B.S., Rao, M.N., Reddy, D.V., Nagabhushanam, P., Hussain, S., Chadha, R.K., Gupta, H.K., 1999. Paleoliquefaction evidence and periodicity of large prehistoric earthquakes in Shillong Plateau, India. Earth Planet. Sci. Lett. 167, 269–282.
Sutar, A.K., Verma, M., Pandey, A.P., Bansal, B.K., Prasad, P.R., Rao, P.R., Sharma, B., 2017. Assessment of maximum earthquake potential of the Kopili fault zone in northeast India and strong ground motion simulation. J. Asian Earth Sci. 147, 439–451.
Szeliga, W., Hough, S., Martin, S., Bilham, R., 2010. Intensity, magnitude, location, and attenuation in India for felt earthquakes since 1762. Bull. Seismol. Soc. Am. 100, 570–584.
Talwani, M., Desa, M.A., Ismaiel, M., Sree Krishna, K., 2016. The tectonic origin of the Bay of Bengal and Bangladesh. J. Geophys. Res. Solid Earth 121, 4836–4851.
Thatcher, W., 1995. Microplate versus continuum descriptions of active tectonic deformation. J. Geophys. Res. Solid Earth 100, 3885–3894.
Toda, S., 2005. Forecasting the evolution of seismicity in southern California: animations built on earthquake stress transfer. J. Geophys. Res. 110.
Valdiya, K., 1976. Himalayan transverse faults and folds and their parallelism with subsurface structures of north Indian plains. Tectonophysics 32, 353–386.
Velasco, A.A., Gee, V.L., Rowe, C., Grujic, D., Hollister, L.S., Hernandez, D., Miller, K.C., Tobgay, T., Fort, M., Harder, S., 2007. Using small, temporary seismic networks for investigating tectonic deformation: brittle deformation and evidence for strike-slip faulting in Bhutan. Seismol. Res. Lett. 78, 446–453.
Vernant, P., Bilham, R., Szeliga, W., Drupka, D., Kalita, S., Bhattacharyya, A., Gaur, V., Pelgay, P., Cattin, R., Berthet, T., 2014. Clockwise rotation of the Brahmaputra Valley relative to India: tectonic convergence in the eastern Himalaya, Naga Hills, and Shillong Plateau. J. Geophys. Res. Solid Earth 119, 6558–6571.
Wang, K., Fialko, Y., 2017. Observations and modeling of coseismic and postseismic deformation due to the 2015 Mw 7.8 Gorkha (Nepal) earthquake. J. Geophys. Res. Solid Earth 123, 761–779. https://doi.org/10.1002/2017JB014620.
Weil, A.B., Yonkee, W.A., 2012. Layer-parallel shortening across the Sevier fold-thrust belt and Laramide foreland of Wyoming: spatial and temporal evolution of a complex geodynamic system. Earth Planet. Sci. Lett. 357, 405–420.
Wells, D.L., Coppersmith, K.J., 1994. New empirical relationships among magnitude, rupture length, rupture width, rupture area, and surface displacement. Bull. Seismol. Soc. Am. 84, 974–1002.
Yeck, W.L., Sheehan, A.F., Anderson, M.L., Erslev, E.A., Miller, K.C., Siddoway, C.S., 2014. Structure of the Bighorn Mountain region, Wyoming, from teleseismic receiver function analysis: implications for the kinematics of Laramide shortening. J. Geophys. Res. Solid Earth 119 (9), 7028–7042.